Co-Expression of Lens Fiber Connexins Modifies Hemi-Gap-Junctional Channel Behavior

L. Ebihara,* X. Xu,* C. Oberti,* E. C. Beyer,# and V. M. Berthoud#

*Department of Physiology and Biophysics, Finch University of Health Sciences/The Chicago Medical School, North Chicago, Illinois 60064, and #Department of Pediatrics, University of Chicago, Chicago, Illinois 60637 USA

ABSTRACT Lens fiber cells contain two gap junction proteins (Cx56 and Cx45.6 in the chicken). Biochemical studies have suggested that these two proteins can form heteromeric connexons. To investigate the biophysical properties of heteromeric lens connexons, Cx56 was co-expressed with Cx45.6 (or its mouse counterpart, Cx50) in *Xenopus* oocytes. Whole-cell and single-channel currents were measured in single oocytes by conventional two-microelectrode voltage-clamp and patch clamp techniques, respectively. Injection of Cx56 cRNA induced a slowly activating, nonselective cation current that activated on depolarization to potentials higher than −10 mV. In contrast, little or no hemichannel current was induced by injection of Cx50 or Cx45.6 cRNA. Co-expression of Cx56 with Cx45.6 or Cx50 led to a shift in the threshold for activation to −40 or −70 mV, respectively. It also slowed the rate of deactivation of the hemichannel currents. Moreover, an increase in the unitary conductance, steady state probability of hemichannel opening and mean open times at negative potentials, was observed in (Cx56 + Cx45.6) cRNA-injected oocytes compared with Cx56 cRNA-injected oocytes. These results indicate that co-expression of lens fiber connexins gives rise to novel channels that may be explained by the formation of heteromeric hemichannels that contain both connexins.

INTRODUCTION

Gap junctional channels allow the intercellular transfer of ions and metabolites between adjacent cells. They are oligomeric assemblies of proteins called connexins (Bruzzone et al., 1996). The functional properties of gap junctional channels composed of one connexin (homomeric/homotypic channels) have been investigated extensively (Barrio et al., 1991; Paul et al., 1991; White et al., 1994; Veenstra et al., 1992). These studies have shown that channels formed from different connexins have distinct gating and permeability properties. However, most cells express more than one connexin (Nicholson et al., 1987; Kanter et al., 1992; Paul et al., 1991) raising the possibility of mixing. One kind of connexin mixing involves heterotypic gap junctional channels in which each hemichannel is composed of a different connexin. Electrophysiological studies have shown that some heterotypic channels exhibit properties that are novel compared with those predicted by examination of the homotypic channels (Barrio et al., 1991; Bruzzone et al., 1994; White et al., 1994). A few studies have also been published in which the data can be interpreted according to a second kind of connexin mixing through the formation of gap junctional channels made of heteromeric connexons (more than one connexin forms the hemichannel) (Barrio et al., 1991; Brink et al., 1997; Bevans et al., 1998).

The lens is an avascular organ in which gap junctions provide a pathway for intercellular communication across the organ supporting cell survival and thus lens transparency. This organ may provide an excellent system to examine the functional consequences of assembly of heteromeric connexons. Three different types of connexins have been identified in the chicken lens: Cx43 (Musil et al., 1990), Cx56 (Rup et al., 1993; Berthoud et al., 1994), and Cx45.6 (Jiang et al., 1994). Cx43 is found exclusively in the epithelial cell layer, whereas Cx56 and Cx45.6 colocalize in lens fiber-fiber gap junctions. Biochemical studies by Konig and Zampighi (1995) and Jiang and Goodenough (1996) suggest that the mammalian lens fiber connexins, Cx46 and Cx50, associate to form heteromeric hemichannels.

In the present study, we have examined the physiological consequences of formation of heteromeric connexons by the lens fiber connexins taking advantage of the ability of some of them to form open hemi-gap-junctional channels in single *Xenopus* oocytes. The data presented in this paper show that co-expression of Cx56 and Cx45.6 or Cx56 and Cx50 induced the formation of functional hemichannels with properties that differ from those expected based on observations of the two homomeric hemichannels.

MATERIALS AND METHODS

Preparation of cRNA

cDNAs encoding chicken Cx45.6 and mouse Cx50 in the pSP64T vector (Krieg and Melton, 1984) were provided by Dr. D. A. Goodenough (Harvard University, Boston, MA). We have previously studied expression of chicken Cx56 (Rup et al., 1993) in *Xenopus* oocytes using the same vector (Ebihara et al., 1995). The constructs were linearized with the restriction enzyme, *Sal*I. cRNAs were transcribed in vitro with SP6 RNA polymerase using the mMessage mMachine (Ambion Inc., Austin, TX). The transcripts were purified on a G-50 Sephadex column (Boehringer

Received for publication 23 January 1998 and in final form 2 October 1998.

Address reprint requests to Dr. Lisa Ebihara, Department of Physiology and Biophysics, Finch University of Health Sciences/The Chicago Medical School, North Chicago, IL 60064. Tel: 847-578-3424; Fax: 847-578-3265; E-mail: ebiharal@mis.finchcms.edu.

0006-3495/99/01/198/09 $2.00

Mannheim, Indianapolis, IN) to remove unincorporated rNTPs and precipitated with isopropanol. The transcripts were then resuspended in diethyl pyrocarbonate-treated water, and aliquots were stored at −80°C. The integrity and yield of RNA were assessed by formaldehyde gel electrophoresis and absorbance at 260 nm, respectively.

Expression of lens connexins in *Xenopus laevis* oocytes

Stage V and VI oocytes were obtained by partial ovariectomy of female *Xenopus laevis* (Nasco, Ft. Atkinson, WI). The oocytes were defolliculated by incubation with collagenase type IA (Sigma Chemical, St. Louis, MO) and injected with oligonucleotides antisense to mRNA for *Xenopus* Cx38 as previously described (Ebihara, 1996). They were stored overnight at 17–18°C in modified Barth's solution (MBS) containing: 88 mM NaCl, 1 mM KCl, 2.4 mM $NaHCO_3$, 15 mM HEPES, 0.3 mM $Ca(NO_3)_2$, 0.41 mM $CaCl_2$, and 0.82 mM $MgSO_4$, pH 7.4. Healthy oocytes were selected and injected with 0.2 to 3 ng RNA and incubated for 12–24 h. To assess levels of expression of homomeric and heteromeric channels, oocytes from a single donor frog were injected with the same amount of each individual connexin cRNA unless otherwise noted and studied at similar times following injection.

For immunoblot analysis of connexins, plasma membrane-enriched preparations were obtained as previously described (White et al., 1994; Gupta et al., 1994; Ebihara et al., 1995). Proteins were resolved by polyacrylamide gel electrophoresis on sodium dodecyl sulfate-containing 9% acrylamide gels and transferred to Immobilon P membrane (Millipore, Bedford, MA). Immunoblots were performed as previously described (Berthoud et al., 1994) using previously characterized rabbit anti-Cx56 antibodies (Berthoud et al., 1994) or anti-Cx45.6 antibodies (kindly provided by Drs. Jean Jiang and Daniel Goodenough; Jiang and Goodenough, 1996). Binding of primary antibodies was detected using alkaline phosphatase-conjugated goat anti-rabbit IgG antibodies (Boehringer Mannheim, Indianapolis, IN) and the nitro blue tetrazolium/BCIP substrate kit (Promega, Madison, WI). For detection of Cx50, a mouse monoclonal antibody kindly provided by Dr. J. Kistler (Kistler et al., 1985) and alkaline phosphatase-conjugated goat anti-mouse Ig (Boehringer Mannheim) were used.

Two-electrode voltage-clamp recording of macroscopic hemi-gap-junctional current

Two-microelectrode voltage-clamp recording of hemi-gap-junctional currents in single oocytes was performed using an Axoclamp 2A or a Geneclamp 500 amplifier (Axon Instruments, Foster City, CA). The current and voltage electrodes had resistances of 0.1–0.2 MΩ, respectively, when filled with 3 M KCl. To prevent KCl from leaking out of the electrodes, the tips of the electrodes were back-filled with a cushion of 1% agar in 3 M KCl (Schreibmayer et al., 1994). The membrane potential was usually recorded differentially between the intracellular electrode and a second electrode located in the bath just outside the oocyte to reduce voltage drops across the series resistance of the external solution. In the low calcium experiments, a bath clamp was used. The current signal was filtered at 20–50 Hz using a 4-pole Bessel filter. Pulse generation and data acquisition was performed using an 80386 computer equipped with PCLAMP6 software and a TL-1 acquisition system (Axon Instruments). All experiments were done at room temperature (22–25°C). Unless otherwise noted, the recordings were performed in MBS containing 0.7 mM Ca^{+2}. Results are presented as mean ± SD.

Single channel current recording

For patch clamp experiments, the vitelline membrane was removed using the technique of Methfessel et al. (1986). Single channel currents were measured from cell-attached and inside-out patches with an Axopatch 200A amplifier (Axon Instruments). Patch pipettes were pulled from Corning #7052 glass capillaries, 1.5 mm (OD)/1.0 mm (ID) (W-P Instruments, New Haven, CT) using a Brown-Flaming Micropipette puller (Sutter Instruments, San Francisco, CA). The patch electrodes were coated with Sylgard (Dow-Corning, Midland, MI) and fire polished. The bath solution contained: 100 mM KCl, 5 mM HEPES, 1 mM EGTA, 1 mM $MgCl_2$, pH 7.4. This solution brought the oocyte's resting potential close to zero. Therefore, the voltages reported here are approximately equal to the actual transmembrane potential. The pipette solution was identical to the bath solution except that TMACl was usually substituted for KCl to eliminate inward flow of current through endogenous stretch activated channels. Current records were filtered at 1 kHz, digitized, and stored on a Tahoe 230 magnetic optical drive (Pinnacle Micro, Irvine, CA) for later analysis.

Single channel analysis

In voltage-step experiments, the ohmic leakage current and uncompensated capacitive current were digitally subtracted using leak templates made from sweeps with no openings. In voltage-ramp experiments, the leak current was digitally subtracted using leak templates constructed from segments of records with no openings. For kinetic analysis of single channels, continuous 2–10 min recordings were idealized using a K-segmental K-means program (written by Dr. Qin, SUNY at Buffalo, Buffalo, NY). A maximal log-likelihood method was used for kinetic modeling of idealized data (Qin et al., 1996; Qin et al., 1997). To verify that the kinetic parameters estimated by this method were valid, the optimized rate constants were used to construct open and closed time histograms and compared with experimentally obtained histograms. Results are presented as mean ± SD.

RESULTS

Co-expression of Cx56 with Cx45.6 or Cx50 modifies the functional behavior of hemi-gap-junctional currents

To verify that the connexins were being efficiently translated and transported to the plasma membrane, immunoblots were performed using oocyte plasma membrane-enriched preparations (Fig. 1). Oocytes injected with Cx45.6 cRNA contained a major anti-Cx45.6 immunoreactive band of an apparent molecular mass (M_r) of 58 kDa (*A*, *lane 1*). Cx56 cRNA-injected oocytes contained the expected Cx56 immunoreactive band of M_r 66 kDa (*B*, *lane 2*). No cross-

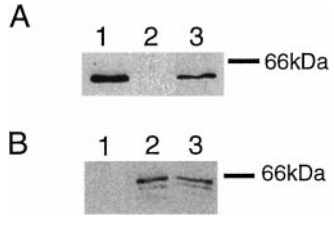

FIGURE 1 Immunoblot analysis of connexin expression in plasma membrane enriched preparations of Xenopus oocytes. Xenopus oocytes were injected with an oligonucleotide antisense to *Xenopus* Cx38 mRNA and Cx45.6 cRNA (*lane 1*), Cx56 cRNA (*lane 2*), or Cx45.6 and Cx56 cRNAs (*lane 3*). Plasma membranes enriched preparations obtained from these oocytes were resolved on sodium dodecyl sulfate-containing 9% polyacrylamide gels, transferred to Immmobilon P and subjected to immunoblotting using anti-Cx45.6 (*A*) or anti-Cx56 (*B*) antibodies. The migration position of the 66.0 kDa is indicated on the right.

reactivity was observed between antibodies and extracts from oocytes injected with the noncorresponding cRNA (*A, lane 2; B, lane 1*). Both proteins were identified in membrane-enriched preparations from oocytes co-injected with cRNA for Cx45.6 and Cx56 (*lane 3*). The presence of Cx50 in oocytes injected with Cx50 cRNA alone or in combination with Cx56 cRNA was similarly confirmed by immunoblot analysis (data not shown).

Macroscopic hemi-gap-junctional currents (I_h) recorded in oocytes injected with cRNA encoding Cx56 or Cx45.6 were compared with currents recorded from oocytes co-injected with cRNA for Cx56 and Cx45.6 using extracellular solutions containing 0.7 mM calcium. Fig. 2 *A* shows families of current traces recorded in response to a series of depolarizing voltage-clamp steps between −30 and +30 mV from a holding potential of −40 mV. Oocytes injected with Cx56 cRNA displayed a large, slowly activating outward current, I_h, which activated at potentials positive to −10 mV as previously reported (Ebihara et al., 1995). No hemi-gap-junctional current was observed in oocytes injected with cRNA for Cx45.6 alone. Co-injection of Cx56 with Cx45.6 induced a slowly activating outward current that had a more negative threshold for activation than Cx56 and a slower rate of deactivation.

The voltage dependence of activation of the hemi-gap-junctional currents was determined by measuring the initial amplitude of the tail current at −40 mV following 24-s prepulses to different potentials. Averaged data showed that the activation curve for I_h in oocytes expressing Cx56 (Fig. 2 *B, open squares*) was shifted to more negative potentials by co-injection with Cx45.6 (Fig. 2 *B, solid circles*). The threshold for activation (the most negative potential at which I_h could be observed) decreased from ~−10 mV ($n = 3$) for oocytes expressing Cx56 to −40 mV ($n = 6$) for oocytes co-expressing Cx56 and Cx45.6. In addition, co-injection of Cx56 with Cx45.6 reduced the slope of the activation curve as might be expected for a heterogeneous population of channels that activate over a wider range of voltages. The magnitude of the hemi-gap-junctional currents in (Cx56 + Cx45.6) cRNA-injected oocytes was significantly smaller than that recorded in oocytes injected with Cx56 alone (Fig. 2 *C*). The outward current (measured at the end of a 24-s step to +30 mV from a holding potential of −40 mV) progressively decreased when the ratio of Cx56 to Cx45.6 subunits was reduced by injecting increasing amounts of Cx45.6 cRNA into the oocytes. The reductions in current suggest that Cx56 associates with Cx45.6 to form heteromers that are less efficiently transported to the cell surface or have reduced function.

Similar but more dramatic changes in gating properties were observed when Cx56 was co-expressed with Cx50. Fig. 3 *A* compares representative families of current traces recorded from oocytes expressing Cx56, (Cx56 + Cx50), or Cx50. Little or no detectable current was present in oocytes injected with Cx50 cRNA alone. Co-expression of Cx50 and Cx56 led to a negative shift in the threshold for acti-

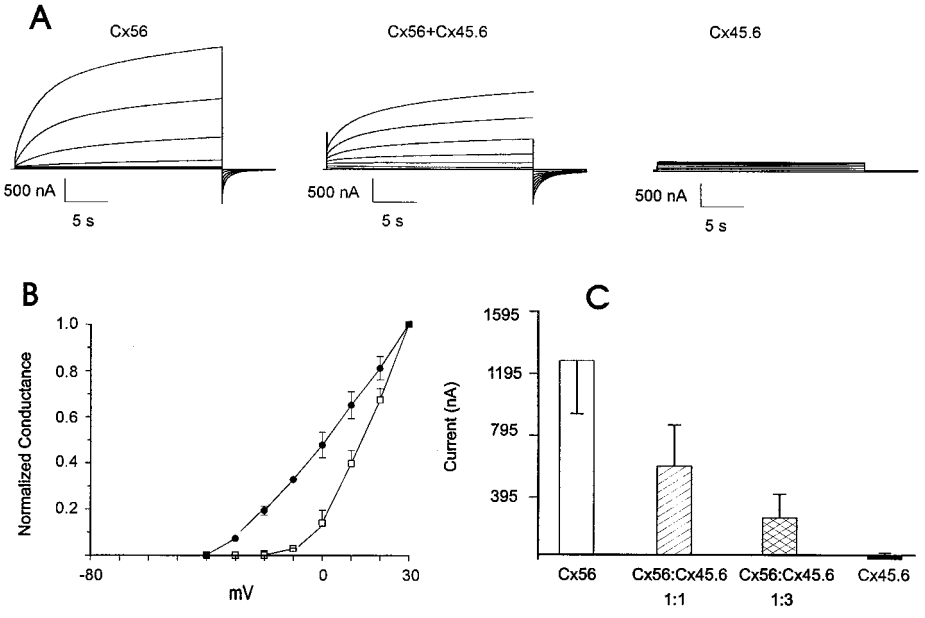

FIGURE 2 Functional expression of Cx56, Cx45.6, and Cx56/Cx45.6 mixtures in *Xenopus* oocytes. (*A*) Membrane currents in response to voltage-clamp steps from −30 mV to +30 mV in 10 mV increments from a holding potential of −40 mV. Approximately equal amounts of each connexin cRNA were injected. (B) Normalized open probability-voltage curves for Cx56 (*open squares*, $n = 3$) and Cx56 + Cx45.6 (*solid circles*, $n = 6$). The normalized open probability was determined by measuring the initial amplitude of the tail current at −40 mV following 24-s prepulses to different potentials and normalizing with respect to the maximum amplitude of the tail current. The initial amplitude of the tail current was obtained by fitting the tail current to a double exponential and extrapolating to zero. (*C*) Mean amplitudes of outward current from oocytes injected with 0.92 ng Cx56 cRNA alone ($n = 6$), 0.92 ng Cx56 and 0.92 ng Cx45.6 cRNA ($n = 4$), 0.92 ng Cx56 and 2.7 ng Cx45.6 cRNA ($n = 6$), or 2.76 ng Cx45.6 cRNA alone ($n = 4$). Currents were measured at the end of a 24-s pulse to +30 mV from a holding potential of −40 mV after correction for a linear leakage component.

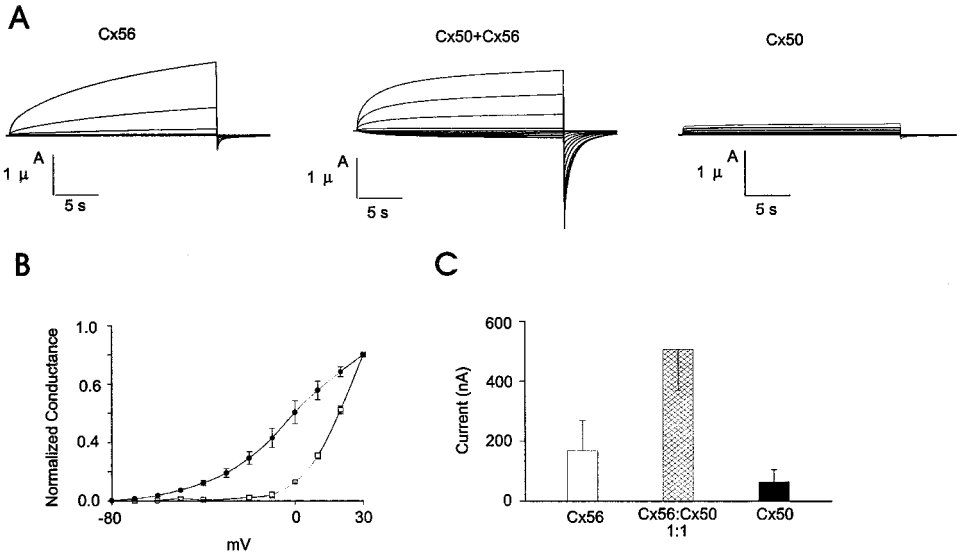

FIGURE 3 Co-expression of Cx50 with Cx56 alters functional properties of hemi-channel currents. (*A*) Membrane currents elicited in response to voltage clamp steps from −70 mV to +30 mV applied in 10 mV (Cx56, Cx56 + Cx50) or 20 mV (Cx50) increments from a holding potential of −80 mV. (*B*) Normalized open probability-voltage curves for cells injected with Cx56 (*open squares*, $n = 3$) and Cx56 + Cx50 (*solid circles*, $n = 4$). The normalized open probability was determined by measuring the initial amplitude of the tail current at −80 mV following 24-s prepulses to different potentials and normalizing with respect to the maximum amplitude of the tail current. The initial amplitude of the tail current was obtained by fitting the tail current to a double exponential and extrapolating to zero. (*C*) Mean amplitudes of the connexin-induced outward current from oocytes injected with 0.92 ng Cx56 cRNA alone ($n = 5$), 0.92 ng Cx50 and 0.92 ng Cx56 cRNA ($n = 4$), or 0.92 ng Cx50 cRNA ($n = 6$). Currents were measured at the end of a 24-s pulse to +20 mV from a holding potential of −40 mV after correction for a linear leakage component.

vation of I_h, accelerated the rate of activation, and slowed the rate of deactivation. Unlike (Cx56 + Cx45.6) oocytes, co-expression of Cx56 and Cx50 increased the amplitude of the resultant hemi-gap-junctional current (measured at the end of a 24-s step to +30 mV from a holding potential of −40 mV) relative to that of Cx56 alone (Fig. 3 *C*). The activation curves for (Cx56 + Cx50)- and Cx56-induced currents are shown in Fig. 3 *B*. (Cx56 + Cx50) channels activated at much more negative voltages and the slope of the activation curve was decreased. The threshold for activation shifted from ~−10 mV for oocytes expressing Cx56 ($n = 3$) to −70 mV for oocytes co-expressing Cx56 and Cx50 ($n = 4$). Furthermore, co-expression of Cx56 with Cx50 reversed the direction of rectification of the instantaneous I-V relationship from outward to inward. This can be observed in Fig. 3 *A* as a marked reduction in the ratio between the activated outward current and the tail current. The ratio between the activated outward current at 30 mV and the initial tail current at −80 mV was 0.19 ± 0.09 ($n = 6$) for oocytes co-expressing Cx56 and Cx50 and 1.6 ± 0.4 ($n = 4$) for oocytes expressing Cx56.

The effect of co-expression of Cx56 with Cx45.6 (or Cx50) on ion selectivity was examined by measuring changes in the reversal potential of I_h when oocytes were exposed to external solutions containing different monovalent cations or anions. The reversal potential was measured using a ramp protocol as previously described (Ebihara and Steiner, 1993). In some experiments, the reversal potential was also estimated from the reversal of I_h on step depolarization or from the reversal of the tail currents. All of these methods gave comparable values for reversal potential. The results of these experiments are summarized in Table 1. Assuming $[Na^+]_i = 20$ mM and $[K^+]_i = 150$ mM (Kusano et al., 1982), in sodium chloride saline (98 mM NaCl), the estimated reversal potential for Na^+ or K^+ in *Xenopus* oocytes would be +40 mV and < −100 mV, respectively. The Cx56 hemi-gap-junctional currents reversed polarity at −12.68 ± 3.6 mV (mean ± SD, $n = 5$) in sodium chloride saline. Replacement of all Na^+ by K^+ shifted E_{rev} to −4.8 ± 2.6 mV (mean ± SD, $n = 4$). Substitution of TMA^+ for Na^+ shifted E_{rev} to −22.0 ± 7.5 mV (mean ± SD, $n = 4$). No significant change in reversal potential was

TABLE 1 Selectivity for cations and anions

	Reversal potential (mean ± SD)			
	NaCl saline*	TMACl saline	KCl saline	Kgluconate saline
Cx56	−12.68 ± 3.6 mV ($n = 5$)	−22.0 ± 7.5 mV ($n = 4$)	−4.8 ± 2.6 mV ($n = 4$)	−4.17 ± 2.4 mV ($n = 3$)
Cx56 + Cx45.6	−14.6 ± 2.5 mV ($n = 6$)	−26.6 ± 0.9 mV ($n = 2$)	−7.6 ± 1.0 mV ($n = 4$)	−5.0 mV ($n = 2$)
Cx56 + Cx50	−10.65 ± 1.5 mV ($n = 2$)	−25.25 ± 0.35 mV ($n = 2$)	−1.25 ± 1.5 mV ($n = 4$)	−3.3 ± 2.9 mV ($n = 3$)

*The bath solution contained 98 mM XY, 0.2–1 mM $CaCl_2$, 1 mM $MgCl_2$ 5 mM HEPES in which X = Na^+, K^+, or TMA^+ and Y = Cl^- or gluconate.

observed when KGluconate was substituted for KCl. These results are in agreement with previous results (Ebihara et al., 1995) and suggest that Cx56 hemi-gap-junctional channels are permeable to monovalent cations and discriminate poorly between Na^+ and K. Co-expression of Cx56 with Cx50 or Cx45.6 did not appear to modify the ionic selectivity of the hemi-gap-junctional channels.

Effect of external calcium

In previous work, reduction of external calcium was shown to increase Cx56 hemi-gap-junctional currents and shift the voltage dependence of activation to more negative potentials (Ebihara et al., 1995). We confirmed this result using Cx56 cRNA-injected oocytes and tested for a similar effect of calcium on Cx45.6 and (Cx56 + Cx45.6) cRNA-injected oocytes. Fig. 4 *A–C* shows the effect of reducing external calcium on macroscopic current traces and I-V curves. Independently of the connexin cRNA injected, reducing the Ca^{2+} concentration to nominally zero caused a marked increase in I_h and shifted the threshold of activation to more negative voltages. However, the Cx45.6- and (Cx56 + Cx45.6)-induced currents activated over a more negative range of potentials than the Cx56-induced current. Furthermore, the Cx45.6-induced currents could only be detected in zero calcium MBS and were considerably smaller in magnitude than the currents induced by injecting oocytes with similar amounts of cRNA for Cx56 or (Cx56 + Cx45.6). No calcium-sensitive membrane currents were observed in control, antisense-treated oocytes (data not shown).

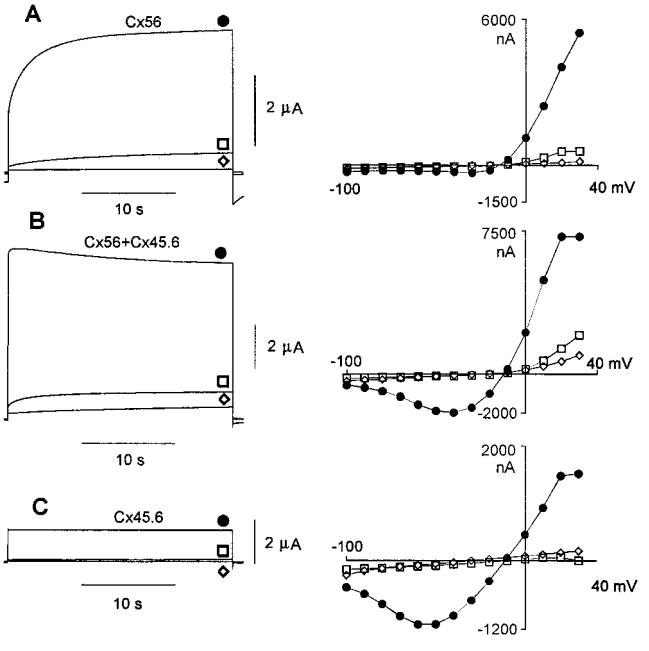

FIGURE 4 Effect of changing external calcium on connexin-induced currents. Macroscopic currents at +20 mV and I-V relationships obtained from oocytes injected with cRNA for Cx56 (*A*), Cx56 + Cx45.6 (*B*), or Cx45.6 (*C*). Hemi-gap-junctional currents were evoked in response to 24-s voltage clamp steps to potentials between −100 and +40 mV from a holding potential of −10 mV in MBS containing 0.7 mM Ca^{+2} (*open squares*) and after superfusion with solutions containing 0 mM Ca^{+2} (*solid circles*) and 3 mM Ca^{+2} (*open diamonds*). I-V relationships were determined by measuring the current at the end of the pulse and plotting it as a function of pulse potential.

The activation and deactivation kinetics and voltage sensitivity of the hemi-gap-junctional currents in zero calcium MBS are shown in greater detail in Fig. 5. Fig. 5 *A* compares families of current traces recorded from oocytes expressing Cx56, (Cx56 + Cx45.6) or Cx45.6 in response to a series of voltage clamp steps between −100 and 20 or 30 mV from a holding potential of −10 mV. In the case of Cx56, the hemichannels were not fully activated at −10 mV and application of depolarizing voltage clamp steps elicited a slowly activating outward current. In the case of Cx45.6 or (Cx45.6 + Cx56), the hemichannels were almost completely activated at −10 mV and application of large depolarizing voltage clamp steps appeared to cause the channels to slowly inactivate. For all the connexins, the hemi-gap-junctional current deactivated with hyperpolarizing steps. However, the Cx56-induced current deactivated more rapidly and to a lower steady-state level than the Cx45.6- or (Cx45.6 + Cx56)-induced currents. To quantitate these differences in steady-state voltage dependence, the rising phase of the normalized steady-state conductance (G_∞) versus voltage curves in zero calcium MBS (Fig. 5 *B*) was fit to a Boltzmann equation of the form:

$$G_\infty = G_{min} + (G_{max} - G_{min})/(1 + \exp(-A * (V - V_o)))$$

The $G_\infty - V$ curve for Cx56 (open squares, $n = 3$) had a midpoint (V_o) of −16.4 mV and a slope factor (A) of 0.11. We were unable to accurately determine the $G_\infty - V$ curve at potentials >30 mV because I_h was contaminated by a large endogenous sodium current. The rising phase of the $G_\infty - V$ curve for Cx45.6 (solid circles, $n = 2$) had a V_o of −65 mV and an A of 0.056. The current was fully activated between −10 and +10 mV and declined at more positive potentials. The $G_\infty - V$ curve for the mixed (Cx45.6 + Cx56) channels had a voltage sensitivity that was intermediate between that of Cx45.6 and Cx56 with a V_o of −45.2 mV and an A of 0.06 (*solid stars*, $n = 2$).

Co-expression of Cx45.6 with Cx56 modifies single hemi-gap-junctional channel gating properties

To investigate the effect of heteromeric assembly on the voltage-dependent gating properties of the hemichannels in more detail, single hemichannel currents produced in (Cx56 + Cx45.6)-injected oocytes were recorded from cell-attached and inside-out patches and compared with those of homomeric Cx56 channels.

An example of single channel currents recorded from a cell-attached patch containing multiple Cx56 channels is shown in Fig. 6 *A*. In this experiment, the membrane potential was initially held at 0 mV, and then a 4-s hyperpolarizing step was applied to the indicated membrane poten-

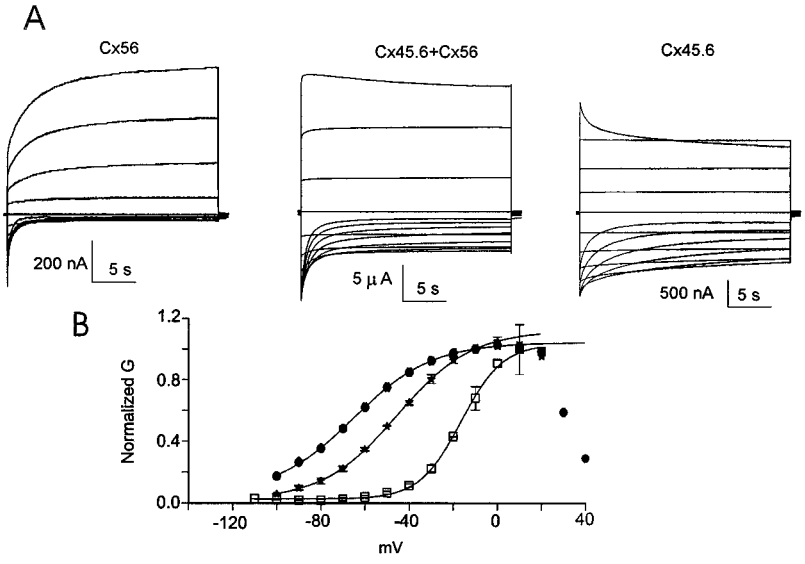

FIGURE 5 Activation and deactivation kinetics and voltage sensitivity of the hemi-gap-junctional currents in zero calcium MBS. (*A*) Hemi-gap-junctional currents recorded from Cx56, (Cx45.6 + Cx56) and Cx45.6 cRNA-injected oocytes in zero calcium MBS. The membrane potential was stepped from −10 mV to a series of voltages between −100 mV and +30 mV (or +20 mV in the case of Cx45.6 + Cx56) in increments of 10 mV. Then 3 mM $CaCl_2$ was added to the external solution and the pulse protocol was repeated. The connexin-induced current shown corresponds to the difference between the current recorded in the absence and presence of calcium. (*B*) Graph of the normalized steady-state conductance (plotted as the ratio of the steady-state current to the initial current) versus voltage relation for Cx56 (*open squares*, $n = 3$), Cx45.6 (*solid circles*, $n = 2$), and (Cx45.6 + Cx56) (*solid stars*, $n = 2$). The solid lines are the best fit of experimental data to a Boltzmann equation with $A = 0.106$, V_o = -16.4 mV, $G_{max} = 1.03$, $G_{min} = 0.02$ for Cx56; $A = 0.056$, $V_o = -65$ mV, $G_{max} = 1.04$, $G_{min} = 0.06$ for Cx45.6; and $A = 0.06$, $V_o = -45.2$ mV, $G_{max} = 1.12$, $G_{min} = 0.02$ for (Cx45.6 + Cx56). The bath contained zero calcium MBS. The hemi-gap-junctional currents were corrected for leakage by subtracting the residual currents recorded in 3 mM calcium. The initial amplitude of the current was obtained by fitting the current trace to the sum of two or three exponentials and extrapolating to zero.

tials. Several channels were open at the beginning of the voltage step. When the membrane potential was stepped to −40 or −60 mV, the channels reopened multiple times before entering a relatively long-lived closed state. The time course of deactivation can be more clearly seen in the ensemble averages obtained from the same patch (Fig. 6 *B*). The effect of voltage on the normalized conductance-voltage curve at 4 s in macropatches is shown in Fig. 6 *C* (*solid circles*). The normalized conductance was estimated by dividing the ensemble averaged current at 4 s by the initial current. The normalized conductance was maximum at potentials between −10 and +40 mV and declined at more negative potentials. At potentials negative to −40 mV, the channels were mostly closed. Comparison of the normalized $G - V$ curve determined from single channel data with the normalized $G - V$ curve determined from macroscopic currents recorded under two-microelectrode voltage-clamp conditions in zero calcium MBS (solid line) demonstrated that the steady-state probability of opening determined by these two methods were in good agreement.

The single channel I-V relationship for Cx56 was determined using a voltage ramp protocol in cell-attached patches. With KCl in the pipette, the I-V relationship was nearly linear and had a slope conductance of ~300 pS (not shown). A similar value for unitary conductance has been previously reported for Cx46 channels at potentials negative to E_{rev} (Trexler et al., 1996). When TMACl was substituted for KCl in the pipette, the I-V relationship became slightly outwardly rectifying with a slope conductance of 163 ± 18.3 pS (mean ± SD, $n = 4$) between −20 and −80 mV and a reversal potential of −19.2 ± 4.8 mV (mean ± SD, $n = 4$) (Fig. 6 *D*).

The kinetics of opening and closing of the Cx56 hemichannels were investigated in more detail at voltages between −30 and −50 mV in several patches containing 1–4 channels. Fig. 7 *A* shows a segment from a typical 10 min, continuous recording at −30 mV. There were at least three channels in this patch. An all-points amplitude histogram of the current distribution from this record (Fig. 7 *B*) shows that the peaks in the amplitude histogram were spaced uniformly with a peak-to-peak current of 4.24 ± 0.09 pA. The channels tended to open as clusters. Within a cluster, there were two types of closures, one brief and the other long lived. This suggests that there are at least two closed states with considerably different mean dwell times. We used a maximum log-likelihood method (Qin et al., 1996) to obtain estimates for mean channel open and closed times as it contains an algorithm for dealing with multiple channels. The simplest scheme that could explain the data contained two closed states and one open state. Open and closed time duration histograms closely followed curves generated using the rate constants indicated in Fig. 7 *C*. The mean open time was 27.2 ms in the experiment shown in Fig. 7. The average mean open time obtained from four other experiments at −40 mV was 23 ± 8.8 ms (mean ± SD).

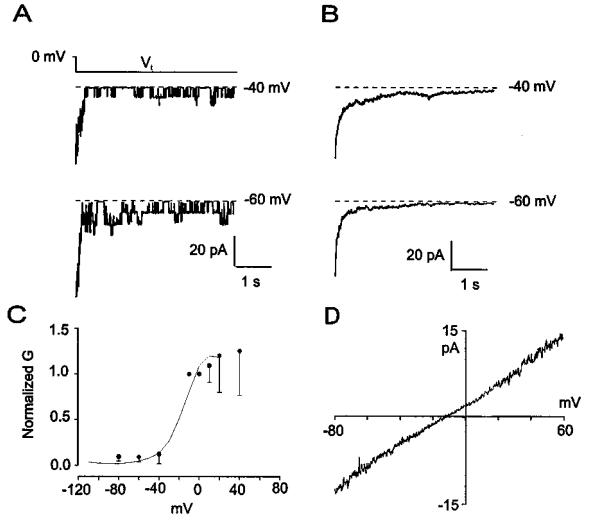

FIGURE 6 (*A*) Single Cx56 hemi-gap-junctional channel currents recorded in a cell-attached patch with voltage steps to −40 mV and −60 mV from a holding potential of 0 mV. The voltage protocol is shown at the top. The data was filtered at 1000 Hz and digitized at 200 μs per point. The dashed lines represent the zero current line. (*B*) Ensemble averages obtained from 40 such records at the indicated potentials. The ensemble averages are expressed as units of current. (*C*) The normalized conductance-voltage relationship determined in macropatches. The normalized conductance was determined by dividing the ensemble averaged current at 4 s by the initial current; $n = 7$. The solid line is the normalized conductance-voltage curve calculated from macroscopic data shown in Fig. 4 by plotting the ratio of the macroscopic current measured at 4 s to the initial current. (*D*) Single channel I-V relationship determined using a ramp protocol. In this protocol, a 10-ms depolarizing pulse was applied to +60 mV followed by a 189-ms ramp from +60 to −80 mV. Data is from a cell-attached patch with 100 mM TMACl saline in the pipette. The slope conductance (determined between −20 and −80 mV) was 184 pS.

To test if co-expression of Cx45.6 and Cx56 affected the single channel characteristics, similar experiments were performed in oocytes co-injected with Cx45.6 and Cx56 cRNA. Representative single channel current traces and open channel I-V relationship are shown in Fig. 8 *A* and *D*. The open channel I-V relationship for (Cx56 + Cx45.6) channels was determined in cell-attached patches using a voltage ramp protocol. With TMACl in the pipette, the slope conductance (determined between −20 and −80 mV) was 206 ± 31.7 pS (mean ± SD, $n = 5$) and the reversal potential was −13.9 ± 2.4 mV (mean ± SD, $n = 5$). This value for single channel conductance was larger than that determined for the Cx56 channels under identical conditions. The variability in the size of the single channels may reflect the existence of many possible heteromeric forms of the channel. Another difference between the Cx56 channels and the (Cx56 + Cx45.6) channels was that the (Cx56 + Cx45.6) channels typically did not deactivate during a 6-s voltage step to −40 or −60 mV; after hyperpolarization, the channel maintained a high probability of opening and underwent only rare transitions to the fully closed state. These single channel properties are reflected in the ensemble averages of (Cx56 + Cx45.6) channel activity (Fig. 8 *B*). The ensemble averaged current had a larger steady-state component. Fig. 8 *C* shows the normalized conductance-voltage curve determined at 6 s from ensemble averaged data. The (Cx56 + Cx45.6) channels activated over a more negative voltage range than the Cx56 channels, and the slope of the curve was less steep. The voltage dependence of the (Cx56 + Cx45.6) channels was nearly identical to that predicted from whole cell recordings (*solid line*).

In addition, we made an attempt to examine the single channel properties of homomeric Cx45.6 channels. Although these experiments were complicated by the fact that the Cx45.6 channels were present in the plasma membrane at a lower density, we were able to successfully record single Cx45.6 channels in two experiments. These channels had a similar conductance, ~220 pS, but were even less sensitive to transmembrane voltage than (Cx56 + Cx45.6) channels (data not shown).

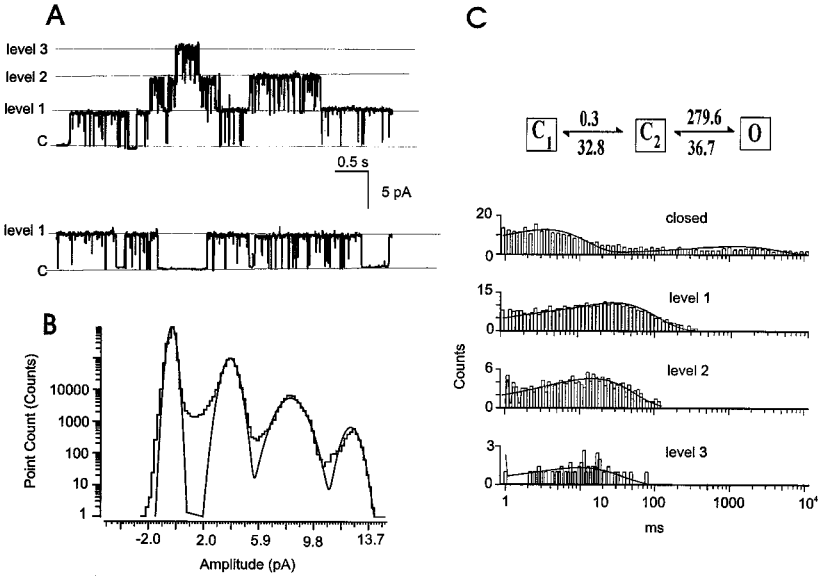

FIGURE 7 (*A*) Currents from single Cx56 hemi-gap-junctional channels at −30 mV. Data is from a cell-attached patch with 100 mM TMACl saline in the pipette. The data was filtered at 1000 Hz and digitized at 200 μs per point. Three levels of opening were observed corresponding to 1 to 3 simultaneously open channels. (*B*) An all-points amplitude histogram of the current distribution of the entire record was fitted to the sum of 4 Gaussians (*smooth line*) with peaks at −0.246, 3.890, 8.188, and 12.465 pA. (*C*) Distributions of closed and open times. The model state diagram with the rate constants (s^{-1}) used to fit the distributions is shown on top. The binned data are from the same patch shown in *A* idealized with a K-segmental K-means method and the continuous lines were calculated directly from the model. There appeared to be four amplitude levels in this experiment corresponding to 0, 1, 2, and 3 simultaneously open channels.

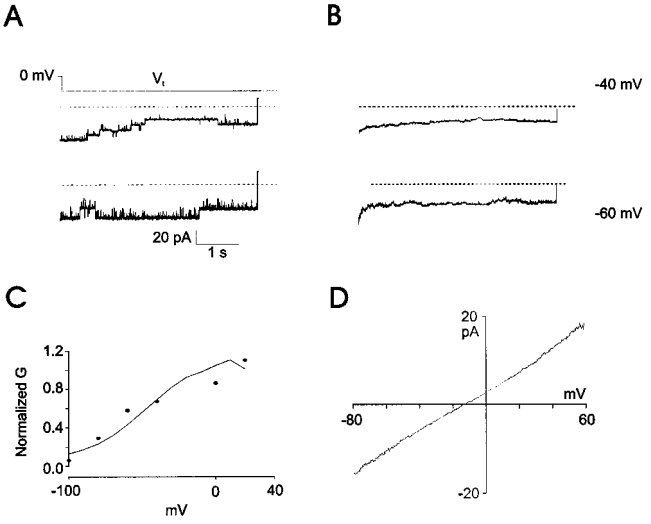

FIGURE 8 (*A*) Single heteromeric (Cx56 + Cx45.6) channel currents recorded in a cell-attached patch with voltage steps to −40 mV and −60 mV from a holding potential of 0 mV. The voltage protocol is shown at the top. The data was filtered at 1000 Hz and digitized at 200 μs per point. The dashed lines represent the zero current line. (*B*) Ensemble averages obtained from eight such records at the indicated potentials. (*C*) Normalized conductance-voltage relationship determined in a macropatch. The normalized conductance was calculated by dividing the ensemble averaged current determined at 6 s by the initial current. The solid line is the normalized conductance-voltage curve calculated from the macroscopic data shown in Fig. 4 by plotting the ratio of the macroscopic current measured at 6 s to the initial current. (*D*) Single channel I-V relationship determined using a ramp protocol. Data is from a cell-attached patch with 100 mM TMACl saline in the pipette. The slope conductance (determined between −20 and −80 mV) was 233 pS in the example shown.

DISCUSSION

In this study we have presented electrophysiological evidence for the formation of heteromeric connexons between the lens fiber connexins, Cx56 and Cx45.6/Cx50. Co-expression of Cx56 with Cx45.6 or Cx50 led to the formation of hemichannels the characteristics of which differed from those of the homomeric connexons. The biochemical data previously published by Konig and Zampighi (1995) and Jiang and Goodenough (1996) support the presence of these heteromeric channels in the lens in vivo.

Previous studies in oocyte pairs have shown that Cx46 is able to form heterotypic gap junctional channels with both Cx43 and Cx50 but that Cx50 does not form functional heterotypic channels when paired with Cx43 (White et al., 1994). In addition, an attempt was made to study heteromeric interactions between Cx46 and Cx50 in the *Xenopus* oocyte pair expression system by pairing oocytes co-injected with Cx46 and Cx50 cRNAs with Cx43-expressing oocytes (White et al., 1994). These experiments demonstrated that oocytes co-expressing Cx46 and Cx50 were able to form functional gap junctional channels with Cx43. Unfortunately, because of the lack of resolution of the two-cell voltage-clamp approach used, the properties of these currents were indistinguishable from those of Cx46/Cx43 oocyte pairs and thus, failed to provide evidence for heteromeric association of Cx46 with Cx50. The approach used in our study was to examine heteromeric interactions more directly by examining the functional properties of hemichannels in single oocytes. Our results show that, whereas Cx56-expressing oocytes can form open hemichannels (Ebihara et al., 1995; and this study), Cx50 or Cx45.6-expressing oocytes show little or no detectable connexin-induced currents in solutions containing 0.7 mM calcium. Thus, if there is no formation of heteromeric connexons, one would expect to record only Cx56-induced currents in oocytes co-injected with Cx56 and Cx50 or Cx45.6. Instead, co-expression of the fiber connexins led to a negative shift in the threshold for activation and slowed the rate of deactivation of the connexin-induced current. It also led to alterations in the magnitude of the current and to an increase in single channel conductance and open times of (Cx45.6 + Cx56) channels compared with Cx56 channels. Co-expression of Cx45.6 (or Cx50) with Cx56 did not result in any obvious changes in ionic selectivity. The ionic selectivity of the hemi-gap-junctional currents was similar to that previously reported for Cx46 (Trexler et al., 1996; Ebihara and Steiner, 1993).

The primary structure of chick Cx45.6 is most similar (>70% amino acid sequence identity) to mouse Cx50 (Jiang et al., 1994; White et al., 1992) and to human Cx50 (Church et al., 1995). Thus, it is not surprising that when chick Cx45.6 and mouse Cx50 are expressed in oocyte pairs, they form homotypic gap junctional channels with similar voltage gating properties (Jiang et al., 1994; White et al., 1992). Nevertheless, our results show that Cx56 associates with Cx45.6 or Cx50 to form heteromeric connexons with distinct electrophysiological properties. In particular, (Cx56 + Cx45.6) channels have a more positive threshold for activation and exhibit a greater degree of outward rectification than (Cx56 + Cx50) channels.

The most important consequence of formation of heteromeric hemi-gap-junctional channels may be of physiological relevance. The mixed channels become less sensitive to block by external calcium or voltage and their mean open times are longer. Thus, the formation of heteromeric hemichannels would tend to increase their contribution to the resting membrane conductance of lens fiber cells. In addition, the formation of heteromeric gap junctional channels in the lens would be expected to alter the ability of lens fiber cells to communicate with each other. The differential properties of heteromeric channels might be crucial for lens transparency, as cataracts form in mice when either of the fiber cell connexins is absent (Gong et al., 1997). But, most importantly, our data suggest a mechanism to explain why autosomal dominant mutations of only one fiber cell connexin, Cx50, (White et al., 1997; Shiels et al., 1998; Steele et al., 1998) can lead to disease. The mutant Cx50 might interfere not only with wild type Cx50 channels, but through heteromeric mixing, it might also interfere with the formation of Cx46 containing channels.

We thank Mary Beth A. Latayan for performing some of the preliminary experiments on (Cx45.6 + Cx56) cRNA-injected oocytes.

This study was supported by the National Institutes of Health Grant EY10589 (to L. Ebihara) and Grant EY08368 (to E. C. Beyer).

REFERENCES

Amman, D., F. Lanter, R. A. Steiner, P. Schulthess, Y. Shijo, and W. Simon. 1981. Neutral carrier based hydrogen ion selective microelectrodes for extra- and intracellular studies. *Anal. Chem.* 53:2267–2269.

Barrio, L. C., T. Suchyna, T. Bargiello, L. X. Xu, R. Roginsky, M. V. L. Bennett, and B. J. Nicholson. 1991. Voltage dependence of homo- and hetero-typic cx26 and cx32 gap junctions expressed in *Xenopus* oocytes. *Proc. Natl. Acad. Sci. USA* 88:8410–8414.

Berthoud, V. M., A. J. Cook, and E. C. Beyer. 1994. Characterization of the gap junction protein connexin56 in the chicken lens by immunofluorescence and immunoblotting. *Invest. Ophthalmol. Vis. Sci.* 35:4109–4117.

Bevans, C. G., M. Kordel, S. K. Rhee, and A. L. Harris. 1998. Isoform composition of connexin channels determines selectivity among messengers and uncharged molecules. *J. Biol. Chem.* 273:2808–2816.

Brink, P. R., K. Cronin, K. Banach, E. Peterson, E. M. Westphale, K. H. Seul, S. V. Ramanan, and E. C. Beyer. 1997. Evidence for heteromeric gap junction channels formed from rat connexin43 and human connexin37. *Am. J. Physiol.* 273:C1386–C1396

Bruzzone, R., T. W. White, and D. L. Paul. 1994. Expression of chimeric connexins reveals new properties of the formation and gating behavior of gap junction channels. *J. Cell Sci.* 107:955–967.

Bruzzone, R., T. W. White, and D. L. Paul. 1996. Connections with connexins: the molecular basis of direct intercellular signaling. *Eur. J. Biochem.* 238:1–27.

Church, R. L., R. H. Wang, and E. Steele. 1995. The human lens intrinsic membrane protein MP70 (Cx50) gene; clonal analysis and chromosome mapping. *Curr. Eye Res.* 14:979–981.

Ebihara, L. 1996. Xenopus Connexin38 forms hemi-gap-junctional channels in the nonjunctional plasma membrane of Xenopus oocytes. *Biophys. J.* 71:742–748.

Ebihara, L., V. M. Berthoud, and E. C. Beyer. 1995. Distinct behavior of connexin56 and connexin46 gap junctional channels can be predicted from the behavior of their hemi-gap-junctional channels. *Biophys. J.* 68:1796–1803.

Ebihara, L., and E. Steiner. 1993. Properties of a nonjunctional current expressed from a rat connexin46 cDNA in Xenopus oocytes. *J. Gen. Physiol.* 102:59–74.

Gong, X., E. Li, G. Klier, Q. Huang, Y. Wu, H. Lei, N. M. Kumar, J. Horwitz, and N. B. Gilula. 1997. Disruption of α_3 connexin gene leads to proteolysis and cataractogenesis in mice. *Cell.* 91:833–843.

Gupta, V. K., V. M. Berthoud, N. Atal, J. A. Jarillo, L. C. Barrio, and E. C. Beyer. 1994. Bovine connexin44, a lens gap junction protein: molecular cloning, immunological characterization, and functional expression. *Invest. Ophthalmol. Vis. Sci.* 35:3747–3758.

Jiang, J. X., and D. A. Goodenough. 1996. Heteromeric connexons in lens gap junction channels. *Proc. Natl. Acad. Sci. USA* 93:1287–1291.

Jiang, J. X., T. W. White, D. A. Goodenough, and D. L. Paul. 1994. Molecular cloning and functional characterization of chick lens fiber connexin 45.6. *Mol. Biol. Cell.* 5:363–373.

Kanter, H. L., J. E. Saffitz, and E. C. Beyer. 1992. Cardiac myocytes express multiple gap junction proteins. *Circ. Res.* 70:438–444.

Kistler, J., B. Kirkland, and S. Bullivant. 1985. Identification of a 70,000-D protein in lens membrane junctional domains. *J. Cell Biol.* 101:28–35.

Konig, N., and G. A. Zampighi. 1995. Purification of bovine lens cell-to-cell channels compoaed of connexin44 and connexin50. *J. Cell Sci.* 108:3091–3098.

Krieg, P. A., and D. A. Melton. 1984. Functional messenger RNAs are produced by SP6 in vitro transcription of cloned cDNAs. *Nucleic Acids Res.* 12:7057–7070.

Kusano, K., R. Miledi, and J. Stinnakre. 1982. Cholinergic and catecholaminergic receptors in the *Xenopus* oocyte membrane. *J. Physiol.* 328:143–170.

Methfessel, C., V. Witzemann, T. Takahashi, M. Mishina, S. Numa, and B. Sakmann. 1986. Patch clamp measurements on *Xenopus laevis* oocytes: currents through endogenous channels and implanted acetylcholine receptor and sodium channels. *Pflugers Arch.* 407:577–588.

Musil, L. S., E. C. Beyer, and D. A. Goodenough. 1990. Expression of the gap junction protein connexin43 in embryonic chick lens: molecular cloning, ultrastructural localization, and post-translational phosphorylation. *J. Membr. Biol.* 116:163–175.

Nicholson, B., R. Dermietzel, D. Teplow, O. Traub, K. Willecke, and J.-P. Revel. 1987. Two homologous protein components of hepatic gap junctions. *Nature.* 329:732–734.

Paul, D. L., L. Ebihara, L. J. Takemoto, K. I. Swenson, and D. A. Goodenough. 1991. Connexin46, a novel lens gap junction protein, induces voltage-gated currents in nonjunctional plasma membrane of *Xenopus* oocytes. *J. Cell Biol.* 115:1077–1089.

Qin, F., A. Auerbach, and F. Sachs. 1996. Estimating single channel kinetic parameters from idealized patch-clamp data containing missed events. *Biophys. J.* 70:264–280.

Qin, F., A. Auerbach, and F. Sachs. 1997. Maximum likelihood estimation of aggregated Markov processes. *Proc. R. Soc. Lond. B Biol. Sci.* 264:375–383.

Rup, D. M., R. D. Veenstra, H.-Z. Wang, P. R. Brink, and E. C. Beyer. 1993. Chick connexin-56, a novel lens gap juncion protein. *J. Biol. Chem.* 268:706–712.

Schreibmayer, W., H. A. Lester, and N. Descal. 1994. Voltage clamping of *Xenopus laevis* oocytes utilizing agarose-cushion electrodes. *Pflugers Arch.* 426:453–458.

Shiels, A., D. Mackay, H. Irisawa, V. Berry, A. Moore, and S. Bhattacharya. 1998. A missense mutation in the human connexin50 gene (GJA8) underlies autosomal dominant "Zonular Pulverulent" cataract, on chromosome 1q. *Am. J. Hum. Genet.* 62:526–532.

Steele, E. C., M. F. Lyon, P. H. Glenister, P. V. Guillot, and R. L. Church. 1998. Identification of a mutation in the Connexin 50 (Cx50) gene of the No2 cataractous mouse mutant. *In* Gap Junctions. Rudolf Werner, editor. IOS Press, Amsterdam. 289–293.

Trexler, E. B., M. V. Bennett, T. A. Bargiello, and V. K. Verselis. 1996. Voltage gating and permeation in a gap junction hemichannel. *Proc. Natl. Acad. Sci. USA* 93:5836–5841.

Veenstra, R. D., H.-Z. Wang, E. M. Westphale, and E. C. Beyer. 1992. Multiple connexins confer distinct regulatory and conductance properties in the developing heart. *Circ. Res.* 71:1277–1283.

White, T. W., R. Bruzzone, D. A. Goodenough, and D. L. Paul. 1992. Mouse cx50, a functional member of the connexin family of gap junction proteins, is the lens fiber protein MP70. *Mol. Biol. Cell.* 3:711–720.

White, T. W., R. Bruzzone, S. Wolfram, D. L. Paul, and D. A. Goodenough. 1994. Selective interactions among the multiple connexin proteins expressed in the vertebrate lens: the second extracellular domain is a determinant of compatibility between connexins. *J. Cell Biol.* 125: 879–892.

White, T. W., D. A. Goodenough, and D. L. Paul. 1997. Ocular abnormalities in connexin50 knockout mice. *Mol. Biol. Cell.* 8:93*a*. (Abstr.)